Clinical & Translational Immunology

Australian and New Zealand Society for Immunology Inc.

Clinical & Translational Immunology 2020; e1224. doi: 10.1002/cti2.1224
www.wileyonlinelibrary.com/journal/cti

ORIGINAL ARTICLE

Innate lymphoid cell composition associates with COVID-19 disease severity

Marina García[1†], Efthymia Kokkinou[1†], Anna Carrasco García[1], Tiphaine Parrot[1], Laura M Palma Medina[1], Kimia T Maleki[1], Wanda Christ[1], Renata Varnaitė[1], Iva Filipovic[1], Hans-Gustaf Ljunggren[1], Niklas K Björkström[1], Elin Folkesson[2,3], Olav Rooyackers[4,5], Lars I Eriksson[5,6], Anders Sönnerborg[2,7], Soo Aleman[2,7], Kristoffer Strålin[2,7], Sara Gredmark-Russ[1,2], Jonas Klingström[1,‡], Jenny Mjösberg[1,‡] & the Karolinska KI/K COVID-19 Study Group

[1]Department of Medicine Huddinge, Center for Infectious Medicine, Karolinska Institutet, Karolinska University Hospital, Stockholm, Sweden
[2]Department of Infectious Diseases, Karolinska University Hospital, Stockholm, Sweden
[3]Department of Medicine Solna, Division of Infectious Diseases, Karolinska Institutet, Stockholm, Sweden
[4]Department of Clinical Science, Technology and Intervention, Division of Anesthesiology and Intensive Care, Karolinska Institutet, Huddinge, Sweden
[5]Function Perioperative Medicine and Intensive Care, Karolinska University Hospital, Stockholm, Sweden
[6]Department of Physiology and Pharmacology, Section for Anesthesiology and Intensive Care, Karolinska Institutet, Stockholm, Sweden
[7]Division of Infectious Diseases and Dermatology, Department of Medicine Huddinge, Karolinska Institutet, Stockholm, Sweden

Correspondence
E Kokkinou, Department of Medicine Huddinge, Center for Infectious Medicine, Karolinska Institutet, Karolinska University Hospital, Stockholm, Sweden.
E-mail: efthymia.kokkinou@ki.se

[†]Joint First authors.
[‡]Joint Senior authors.

Received 12 October 2020;
Revised 16 November 2020;
Accepted 16 November 2020

doi: 10.1002/cti2.1224

Clinical & Translational Immunology
2020; **9**: e1224

Abstract

Objectives. The role of innate lymphoid cells (ILCs) in coronavirus disease 2019 (COVID-19), caused by severe acute respiratory syndrome coronavirus 2 (SARS-CoV-2), is unknown. Understanding the immune response in COVID-19 could contribute to unravel the pathogenesis and identification of treatment targets. Here, we describe the phenotypic landscape of circulating ILCs in COVID-19 patients and identified ILC phenotypes correlated to serum biomarkers, clinical markers and laboratory parameters relevant in COVID-19. **Methods.** Blood samples collected from moderately ($n = 11$) and severely ill ($n = 12$) COVID-19 patients, as well as healthy control donors ($n = 16$), were analysed with 18-parameter flow cytometry. Using supervised and unsupervised approaches, we examined the ILC activation status and homing profile. Clinical and laboratory parameters were obtained from all COVID-19 patients, and serum biomarkers were analysed with multiplex immunoassays. **Results.** Innate lymphoid cells were largely depleted from the circulation of COVID-19 patients compared with healthy controls. Remaining circulating ILCs revealed decreased frequencies of ILC2 in severe COVID-19, with a concomitant decrease of ILC precursors (ILCp) in all patients, compared with controls. ILC2 and ILCp showed an activated phenotype with increased CD69 expression, whereas expression levels of the chemokine receptors CXCR3 and CCR4 were significantly altered in ILC2 and ILCp, and ILC1, respectively. The activated ILC profile of COVID-19 patients was associated with soluble inflammatory

markers, while frequencies of ILC subsets were correlated with laboratory parameters that reflect the disease severity. **Conclusion.** This study provides insights into the potential role of ILCs in immune responses against SARS-CoV-2, particularly linked to the severity of COVID-19.

Keywords: coronavirus, COVID-19, immune response, innate lymphoid cells, respiratory viral infection, SARS-CoV-2

INTRODUCTION

Coronavirus disease 2019 (COVID-19), caused by the novel severe acute respiratory syndrome coronavirus 2 (SARS-CoV-2), is of global concern, and major efforts to identify effective treatments and vaccines are currently underway.[1–4] SARS-CoV-2 affects mainly the respiratory tract, and infected individuals often manifest flu-like symptoms. While some patients recover within weeks, others progress to a severe stage of disease, typically including severe respiratory distress and hypoxia with later multi-organ failure, occasionally leading to death.[5,6] Notably, a gradual progression to more severe disease stages coincides with the development of a hyperactivated immune response, triggering a systemic cytokine storm circulatory impairment, sometimes leading to circulatory shock.[7–9] Thus, there are reasons to believe that immunopathology involving the innate immune system plays a potent role behind severe morbidity and mortality in the critically ill COVID-19 patients. Currently, little information is available on the role of innate immune cells in COVID-19. Therefore, here we studied the role of innate lymphoid cell (ILC) in hospitalised COVID-19 patients.

Innate lymphoid cells are innate lymphocytes which, unlike T and B cells, lack rearranged antigen-specific receptors and cell surface markers associated with other lymphoid and myeloid lineages.[10] ILCs are categorised into five major groups: natural killer (NK) cells, ILC1, ILC2, ILC3 and lymphoid tissue inducer (LTi) cells.[10] Based on their transcription factor dependence and functional characteristics, ILC1,[11,12] ILC2[13–15] and ILC3[16] are considered the innate counterparts of the specialised subsets of $CD4^+$ T cells, that is Th1, Th2 and Th17 cells, respectively, while NK cells mirror the cytotoxic functions of $CD8^+$ T cells.[10] Although ILCs exert their function primarily in tissues, distinct subsets of ILCs are found circulating in blood.[17,18] The major blood ILC population is the ILC precursor (ILCp), with the capacity to home to peripheral tissues and differentiate to mature ILC subsets.[18] However, human blood also harbours the committed ILC lineages ILC1 and ILC2. ILC2 in blood express CRTH2 and CD161 and are dependent on the GATA binding protein-3 (GATA-3) transcription factor.[19] IFN-γ-producing ILCs, reminiscent of ILC1, have been identified in peripheral blood.[20] While their characterisation has been challenging because of the lack of unique surface markers,[21] studies have shown that blood ILC1 that produce IFN-γ express the chemokine receptor CXCR3.[20] Hence, CXCR3 serves as a marker to define the ILC1 subset in peripheral blood.

While little is known regarding ILCs in the context of human respiratory viral infections, studies performed in mice highlight their contribution during acute viral infection. More specifically, ILC2 have been suggested to accumulate in the lung of influenza virus-infected mice and promote lung homeostasis and tissue repair.[22] In contrast, ILC2, in concordance with T cells, were reported to contribute to allergic airway inflammation induced by influenza virus in mice.[23] In humans, ILCs have been investigated in acutely HIV-1-infected individuals where they were found to be depleted from the circulation.[24] To the best of our knowledge, ILCs have not yet been investigated in a human respiratory viral disease.

Understanding the immunopathogenesis of COVID-19 is urgently needed in order to help tackle the current pandemic. In the present study, we report a profound reduction in number of ILCs within the systemic circulation of COVID-19 patients. The remaining ILCs show dysregulated expression of markers associated with activation and migration. Furthermore, ILC frequencies are correlated to clinical parameters related to COVID-19 disease severity.

RESULTS

A total of 23 patients with either moderate ($n = 11$) or severe ($n = 12$) COVID-19 and 16 control donors were included in the study (Figure 1a). The COVID-19 patients showed profound perturbations in inflammatory markers, coagulation factors, organ/muscle damage markers and biochemical, haematological and serological parameters (Supplementary figure 1). A detailed summary of the patients' clinical and laboratory parameters is presented in Tables 1 and 2. A timeline summarising the major clinical events of the patients is shown in Figure 1b.

For the identification and analysis of peripheral blood ILCs, we used 18-parameter flow cytometry and a modification of a well-established gating strategy[25] (Supplementary figure 2a). We found that the relative frequencies and absolute counts of total CD127$^+$ ILCs (hereafter referred to as total ILCs), as well as the absolute counts of the specific subsets ILC1, ILC2 and ILCp, were decreased in peripheral blood of moderate and severe COVID-19 patients, while ILC2 counts were only reduced in severe, and not moderate, COVID-19 as compared with controls (Figure 2a–d). Further characterisation of the remaining circulating ILC compartment showed reduced ILCp frequencies in COVID-19 patients, while the frequencies of ILC1 remained unchanged (Figure 2c and e). Of note, the moderately ill group showed elevated frequencies of both total ILC2 (Figure 2e) and CD117$^-$ ILC2, as compared with the control group (Figure 2f).

Taken together, we observed a general ILC depletion as well as compositional changes in the circulating ILC compartment of COVID-19 patients. Interestingly, changes in the relative frequency of ILCs differed between the moderate and severe groups, prompting a more detailed phenotypical study of the ILCs.

To deepen our understanding of the differentiation, activation and migration of ILCs during COVID-19, we assessed differentiation (CD56 and NKp44) (Supplementary figure 3a) and activation (CD69, HLA-DR and Ki-67) markers as well as chemokine receptors (CCR4, CCR6 and CXCR3) and molecules associated with naivety and homing to lymphoid tissues (CD45RA and CD62L) on ILCs (Figure 3a–h). Manual gating and unbiased principal component analysis (PCA) were used to simultaneously take into account the relative frequency of all the markers measured on ILCs.

This approach revealed a higher relative frequency of CD69-expressing total ILCs in patients as compared with controls (Figure 3a). Additionally, Ki-67, a marker of cell proliferation, was increased in severe compared with moderate COVID-19 but decreased in moderate COVID-19 compared with controls (Figure 3a). However, the overall Ki-67 expression level was low in all ILCs regardless of the study group, suggesting either a low proliferating capacity of ILCs in peripheral blood or migration of proliferative ILCs to tissues at an earlier stage. In line with an increase in CD69 in COVID-19 patients, we detected reduced frequencies of total ILCs expressing CD45RA and CD62L, two markers associated with ILC naivety,[18] in severe COVID-19 patients (Figure 3a). Additionally, we observed alterations in chemokine receptor expression between controls and moderate COVID-19 patients, revealing a reduction in the percentage of CXCR3$^+$ and an increase in CCR4$^+$ ILCs. The latter likely reflects the increase in ILC2 frequencies in these patients (Figure 2e), as CCR4 is particularly highly expressed on ILC2 (Figure 3e). Despite these changes in ILC phenotypes, the PCA could not discriminate between COVID-19 patients and controls on the basis of the total ILC data (Figure 3b), suggesting that the COVID-19-related changes in total ILCs are ILC subset specific.

Indeed, we observed no changes in expression of markers associated with differentiation and activation in ILC1. There was, however, a slightly increased percentage of CCR4$^+$ ILC1 cells in COVID-19 patients compared to controls (Figure 3c). We also detected a reduction of CD56$^+$ ILC1 in COVID-19 patients (Supplementary figure 3a). PCA illustrated these differences well, showing segregation of the ILC1 data on the basis of CCR4 for COVID-19 patients and CD56 for controls (Figure 3d).

In contrast, ILC2 displayed an activated phenotype in COVID-19 patients, showing higher frequencies of CD69$^+$ and a tendency towards reduced frequencies of CD62L$^+$ cells, as compared with controls (Figure 3e). Interestingly, Ki-67, generally expressed at very low levels, was decreased in relative frequency in ILC2 from severe COVID-19 patients compared to the control group, possibly reflecting tissue recruitment of such cells in severe COVID-19. Indeed, we

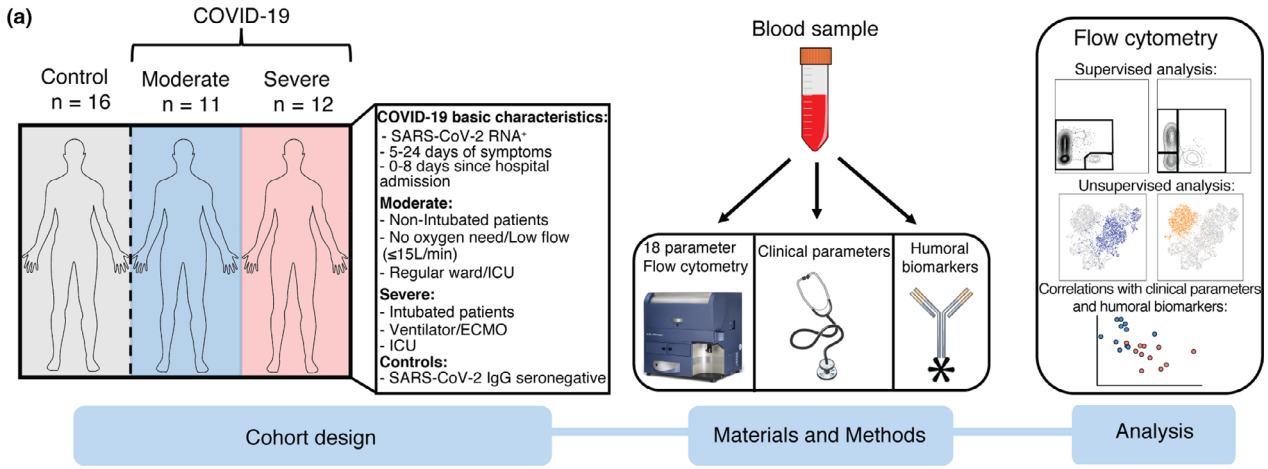

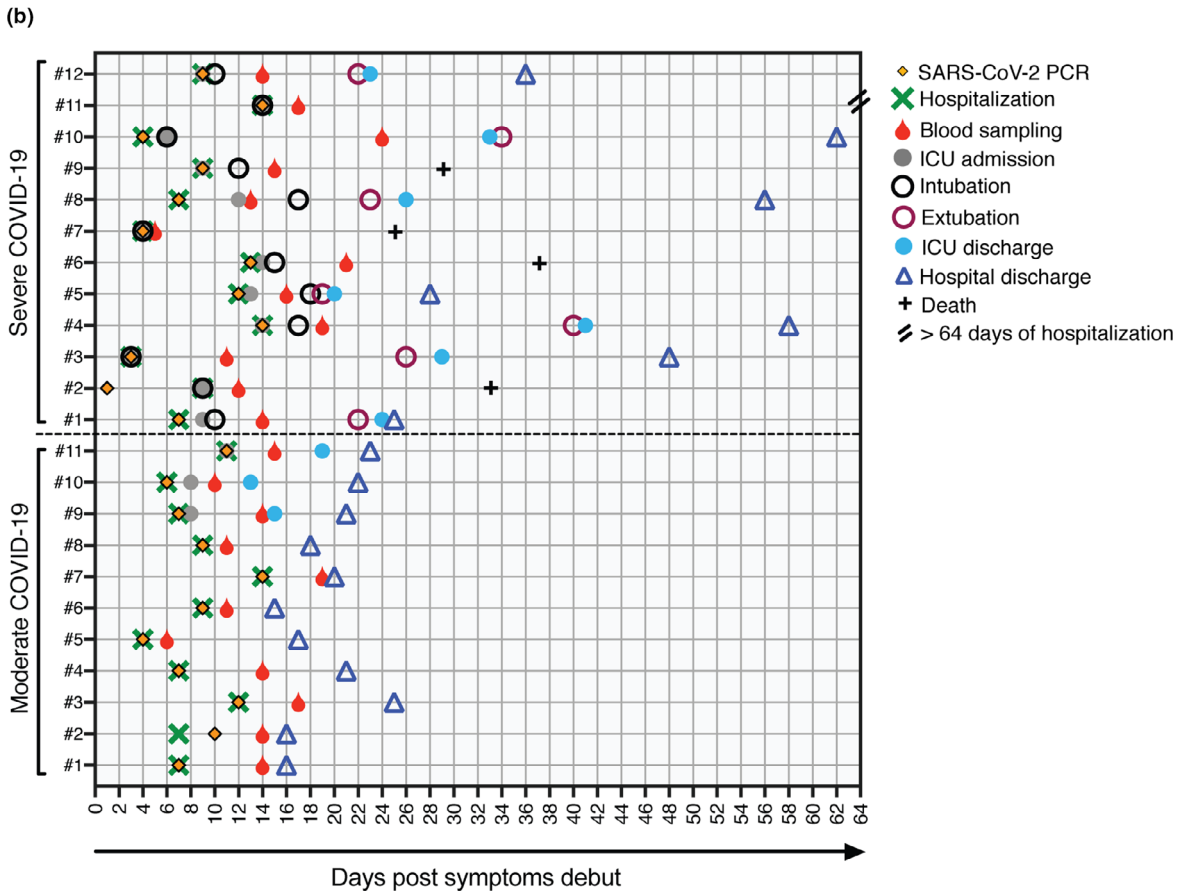

Figure 1. Experimental design and COVID-19 cohort characteristics. **(a)** Schematic representation of the cohort characteristics (left), materials and methods (middle) and the type of analysis performed using the flow cytometric data (right). **(b)** Graphical overview of all COVID-19 patients (n = 23) illustrating clinical events from the day of symptom debut. Depicted are the day of the SARS-CoV-2 PCR test, hospitalisation and blood sampling. For all the severe patients and three of the moderate patients, the day of the intensive care unit (ICU) admission and discharge is indicated. Furthermore, the day of intubation/extubation of the severe patients is shown. Lastly, depicted is the day of hospital discharge for 22 out of 23 patients and the number of deceased patients (n = 4). One patient from the severe group (#11) is still in ECMO with ongoing hospitalisation (> 64 days).

Table 1. Donor characteristics

	Controls (n = 16)	COVID-19 moderate (n = 11)	COVID-19 severe (n = 12)
Risk factors			
Age, median (range)	54 (34–69)	56 (18–67)	59.5 (40–74)
Gender, male, *n* (%)	10 (62.5)	7 (63.6)	10 (83.3)
BMI[a], median (range)	n/a	27 (23–35.06)	29.5 (23–55)
Smoker (Yes/No/Prior/Unclear, %)	n/a	10/36/27/27	8.3/58.3/25/8.3
Pre-existing pathologies			
Asthma, *n* (%)	n/a	1 (9)	2 (16.6)
Diabetes Type 2, *n* (%)	n/a	1 (9)	1 (8.3)
Hypertension, *n* (%)	n/a	2 (18)	4 (33.3)
Coronary heart disease, *n* (%)	n/a	1 (9)	0 (0)
Viraemia at time of sampling, *n* (%)	n/a	2 (18)	7 (58.3)
Symptoms on admission			
Fever, *n* (%)	n/a	11 (100)	12 (100)
Cough, *n* (%)	n/a	10 (91)	11 (91.6)
Dyspnoea, *n* (%)	n/a	11 (100)	12 (100)
Body ache, *n* (%)	n/a	6 (54.5)	6 (50)
Gastrointestinal, *n* (%)	n/a	2 (18)	2 (16.6)
Days from symptom debut to admission, median (range)	n/a	7 (4–14)	9 (3–14)
Days from symptom debut to sampling, median (range)	n/a	14 (6–19)	14 (5–24)
Peak oxygen need			
None, *n* (%)	n/a	2 (18)	0 (0)
Low flow < 10 L min^{-1}, *n* (%)	n/a	5 (45.4)	0 (0)
Low flow 10–15 L min^{-1}, *n* (%)	n/a	4 (36.4)	0 (0)
Ventilator, *n* (%)	n/a	0 (0)	12 (100)[b]
PaO_2/FiO_2 ratio, median mmHg (range)	n/a	323 (112–523)	136 (52–192)
Duration of oxygen treatment in days, median (range)	n/a	7 (0–13)	22 (7–33), 1 still ongoing
Treatments prior to sampling			
Anti-coagulant, (Low-molecular-weight heparin), *n* (%)	n/a	11 (100)	11 (91.6), 1 unclear
Corticosteroids, *n* (%)	n/a	4 (36.4)	8 (66.6)
Antibiotics, *n* (%)	n/a	5 (45.4), all Cefotaxim	7 (58.3) Cefotaxim, 1 (8.3) all the above
Antiviral/Cytokine inhibitors, *n* (%)	n/a	0 (0)	2 (16.6): Remdesivir, Tocilizumab
Laboratory testing			
PCR positivity in nasopharynx/sputum, *n* (%)	n/a	11 (100), n = 1 sputum	12 (100), all nasopharynx
PCR positivity in serum, *n* (%)	n/a	2 (18)	7 (58.3)
Antibody reactivity, *n* (%)	0 (0)	7 (63.3) reactive, 1 (9) gray zone	11 (91.6) reactive, 1 (8.3) gray zone
Neutralizing antibody titres, median (range)	0 (0)	960 (0–2560)	1440 (60–5120)
Clinical course			
Days in ICU from admission until discharge, median (range)	n/a	For 3/11 patients: 7 (5–8)	For 11/12: 18 (7–27), 1 ongoing
Days of intubation, median (range)	n/a	0 (0), n = 3 n/a	18 (1–28), 1 ongoing
Days hospitalized, median (range)	n/a	11 (6–14)	22 (16–58), 1 ongoing
Radiological bilateral infiltrations, *n* (%)	n/a	6 (54.5), n = 5 n/a	12 (100)
Positive culture findings in blood ± 5 days from sampling, *n* (%)	n/a	0 (0)	4 (33.3)
Positive culture findings in lower respiratory tract ± 5 days from sampling, *n* (%)	n/a	0 (0)	7 (58.3)
Pulmonary embolism, *n* (%)	n/a	0 (0)	2 (16.6)
Outcome			
Discharged, *n* (%)	n/a	11 (100)	8 (66.6)
Deceased, *n* (%)	n/a	0 (0)	4 (33.3)

[a]BMI: body mass index (18.5–24.9 normal; 25–29.9 overweight; > 30 obesity).
[b]n = 1 patient in ECMO, n/a: not available.

Table 2. Laboratory parameters of COVID-19 patients

	Reference	COVID-19 Moderate (n = 11) Median peak (range)	COVID-19 Severe (n = 12) Median peak (range)	P-value
Before study sampling				
C-reactive protein, mg L^{-1}	< 3	176 (34–346)	310 (124–452)	**0.0268**
Procalcitonin, μg L^{-1}	< 0.5	0.4 (0.11–66)	1.2 (0.19–10)	0.1335
D-dimer, mg L^{-1}	< 0.56	0.88 (0.33–1.5)	2.5 (0.9–5.4)	**< 0.0001**
Ferritin, μg L^{-1}	10–150	866 (222–2293)	1946 (305–5500)	**0.0156**
Fibrinogen, g L^{-1}	2–4.2	6.1 (4.9–10.2), n = 8 n/a	7.2 (4.1–9.6)	0.8066
Lactate dehydrogenase, μkat L^{-1}	< 3.5	5.7 (0.89–13.7)	10.9 (7–23)	**0.0002**
Alanine aminotransferase, μkat L^{-1}	< 0.76	0.8 (0.51–3.43)	1.31 (0.67–2.52)	0.3788
Bilirubin, μmol L^{-1}	< 26	8 (4–15)	12 (7–81)	**0.0063**
Creatinine, μmol L^{-1}	< 90	77 (46–96)	87 (54–326)	0.0938
Prothrombin complex, INR	< 1.2	1 (0.9–1.1)	1.1 (1–1.4)	**0.0077**
Troponin T, ng L^{-1}	< 15	9.5 (5–19), n = 1 n/a	19 (5–601)	**0.0159**
Myoglobin, μg L^{-1}	< 73	36.5 (22–158), n = 5 n/a	658 (46–6400)	**0.0008**
Lymphocytes, lowest, × 10^9 L^{-1}	1.1–3.5	0.7 (0.3–1.9)	0.5 (0.2–1.1)	0.1443
Neutrophils, lowest, × 10^9 L^{-1}	1.6–5.9	3.7 (0.5–6.5)	6.3 (3.3–15.9)	**0.0195**
Platelets, lowest, × 10^9 L^{-1}	165–387	228 (131–342)	212 (115–315)	0.7980
Platelets, highest, × 10^9 L^{-1}	165–387	401 (152–659)	427.5 (214–770)	0.7399
At study sampling (± 24 h)				
C-reactive protein, mg L^{-1}	< 3	103 (20–394), n = 1 n/a	258 (51–346)	**0.0249**
Procalcitonin, μg L^{-1}	< 0.5	0.36 (0.12–866), n = 2 n/a	0.945 (0.16–10)	0.3358
D-dimer, mg L^{-1}	< 0.56	0.60 (0.36–1.56), n = 1 n/a	3.7 (0.74–7.6)	**0.0002**
Ferritin, μg L^{-1}	10–150	847 (161–2370)	1852 (312–4306), n = 1 n/a	**0.0336**
Fibrinogen, g L^{-1}	2–4.2	4.9 (4.7–10.2), n = 8 n/a	7.4 (4.1–9.6), n = 1 n/a	0.6786
Bilirubin, μmol L^{-1}	< 26	6 (0–11)	9 (6–81)	**0.0011**
Creatinine, μmol L^{-1}	< 90	69 (36–78)	73.5 (44–326)	0.2536
Haemoglobin, g L^{-1}	117–153	118 (90–145)	112.5 (84–146)	0.5553
P-Albumin, g L^{-1}	36–48	27 (21–37), n = 4 n/a	18 (16–22)	**0.0188**
Prothrombin complex, INR	< 1.2	1.05 (0.9–1.1), n = 5 n/a	1.1 (0.9–1.4)	0.0980
Troponin T, ng L^{-1}	< 15	7.5 (5–10), n = 3 n/a	17.5 (5–434)	**0.0325**
Lymphocytes, lowest, × 10^9 L^{-1}	1.1–3.5	1.3 (0.3–2.4)	0.65 (0.3–1.8)	**0.0231**
Neutrophils, highest, × 10^9 L^{-1}	1.6–5.9	4.6 (0.9–9.3)	11.2 (8.5–16.7)	**< 0.0001**
Platelets, lowest, × 10^9 L^{-1}	165–387	345.5 (131–642), n = 1 n/a	363 (179–502)	0.9876
Leukocytes, highest, × 10^9 L^{-1}	3.5–8.8	7.1 (1.5–12.6)	12.6 (9.2–18.4)	**0.0001**
Leukocytes, lowest, × 10^9 L^{-1}	3.5–8.8	6.7 (1–10.5)	9.8 (7.6–15.7)	**0.0003**
At study sampling (± 5 days)				
Interleukin-6, ng L^{-1}	< 7	62 (2–150), n = 2 n/a	472.5 (33–8093)	**0.0035**

P-value: Mann–Whitney U-test, n/a: not available.
The bold values indicate statistical significance according to the following: *P < 0.05, **P < 0.01, ***P < 0.001.

identified dysregulated chemokine receptor expression on ILC2 in COVID-19 patients, specifically CXCR3 and CCR6 which was significantly reduced in the patients as compared with controls (Figure 3e, Supplementary figure 3b). PCA provided an illustration of these findings by segregating the ILC2 data from patients and controls based on CD69 expression for patients and chemokine receptors as well as CD62L and CD45RA for the controls (Figure 3f). The latter two were, however, not statistically different between the groups (Figure 3e).

ILCp showed an activated profile in COVID-19 patients, with increased CD69 and HLA-DR expression as compared with controls. Additionally, CXCR3 was decreased on ILCp in COVID-19 patients as compared with controls (Figure 3g). Although PCA did not separate the ILCp phenotype from patients and controls clearly, there was a tendency towards separation of ILCp from controls on the basis of CD62L and CD45RA (Figure 3h). These two markers showed reduced tendency but were not statistically significant in the manual gating (Figure 3g).

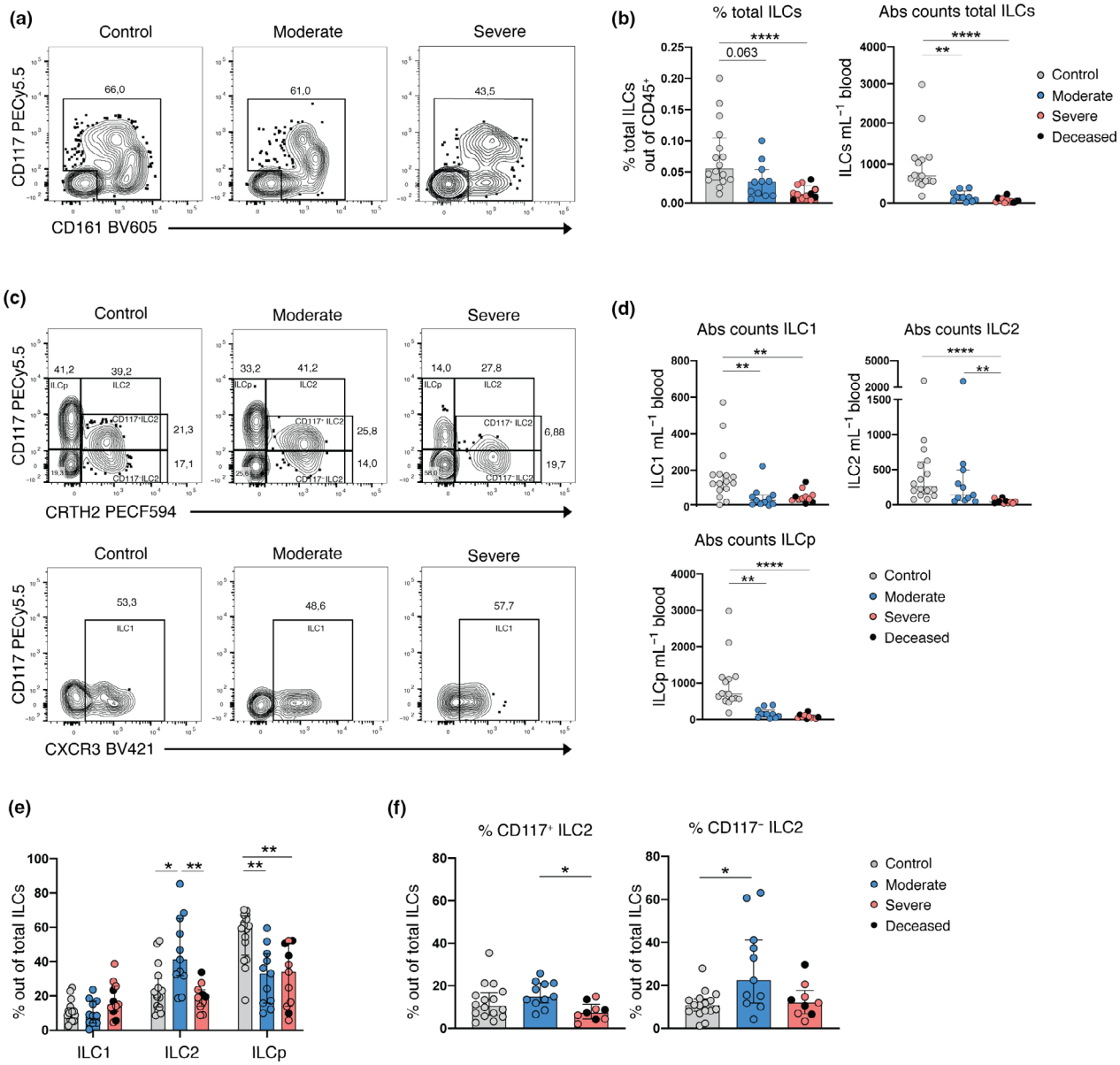

Figure 2. Depletion and altered frequency of ILCs in the peripheral blood of COVID-19 patients. **(a)** Representative flow cytometry plots depicting the gate for the identification of the total ILCs in one control donor, one moderate and one severe COVID-19 patient. **(b)** Bar plot summaries of the percentage (left) and absolute counts (per mL of blood) (right) of total ILCs in control donors (n = 16), moderate (n = 11) and severe (n = 12) COVID-19 patients. **(c)** Representative flow cytometry plots depicting total ILCs gated as: ILCp, ILC2 ($CD117^{+}/^{-}$) (upper row) and ILC1 (lower row) in one control donor, one moderate and one severe COVID-19 patient. **(d)** Bar plot summaries of absolute counts of ILC1, ILC2 and ILCp subsets (per mL of blood) in control donors (n = 16), moderate (n = 11) and severe (n = 11) COVID-19 patients. **(e)** Bar plot summaries of the percentage of ILC1, ILC2 and ILCp of total ILCs in control donors (n = 16), moderate (n = 11) and severe (n = 11) COVID-19 patients. **(f)** Bar plot summaries of the percentage of $CD117^{+}$ and $CD117^{-}$ ILC2 of total ILCs in control donors (n = 16), moderate (n = 11) and severe (n = 9) COVID-19 patients. **(b, d, e, f)** Statistical differences were tested using the Kruskal–Wallis test followed by Dunn's multiple comparisons test. Numbers in flow cytometry plots indicate percentage of cells within the mother gate. Bar graphs are shown as median ± IQR, $^{*}P < 0.05$, $^{**}P < 0.01$, $^{***}P < 0.001$. Patients with low cell numbers (fewer than 20 events) in the corresponding gate were removed from the analysis.

Overall, these findings suggest that the ILCs remaining in the circulation of COVID-19 patients are activated and show an altered expression of chemokine receptors, particularly a decrease in CXCR3, possibly reflecting alterations in CXCR3-ligand-dependent ILC recruitment to tissues.

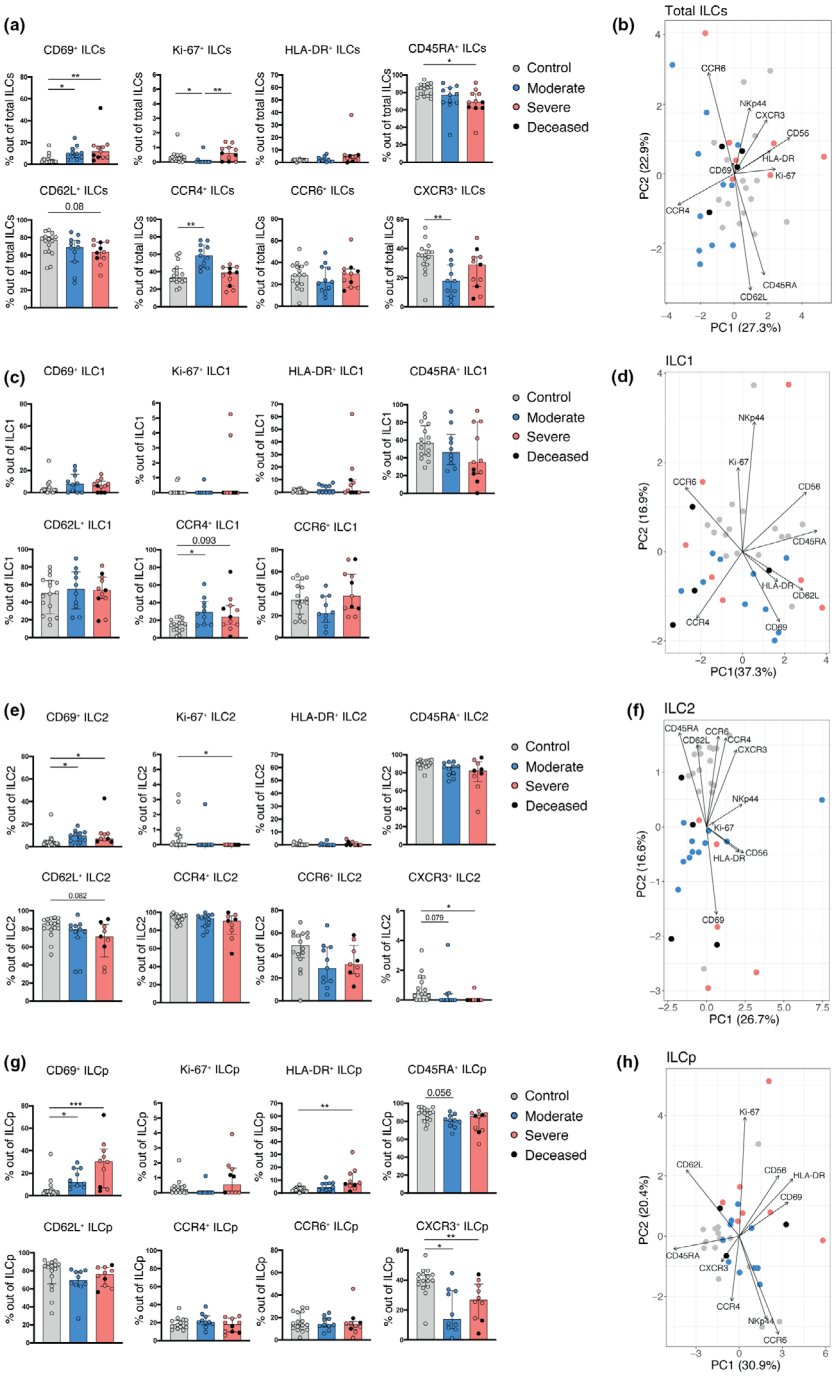

Figure 3. ILCs reveal an activated and migratory profile in peripheral blood of COVID-19 patients. **(a)** Bar plot summaries showing the percentages of the indicated markers in total ILCs in control donors (n = 16), moderate (n = 11) and severe (n = 11) COVID-19 patients. **(b)** PCA plot of total ILCs from control donors (n = 16), moderate (n = 11) and severe (n = 11) COVID-19 patients based on the cell surface markers presented in **(a)**. **(c)** Bar plot summaries showing the percentages of the indicated markers in the ILC1 subset in control donors (n = 16), moderate (n = 10) and severe (n = 11) groups. **(d)** PCA plot of ILC1 showing the contribution of cell surface markers indicated in **(c)**. **(e)** Bar plot summaries showing the percentages of the indicated markers in the ILC2 subset in control donors (n = 16), moderate (n = 11) and severe (n = 9) groups. **(f)** PCA plot of ILC2 showing the contribution of cell surface markers indicated in **(e)**. **(g)** Bar plot summaries showing the percentages of the indicated markers in the ILCp subset in control donors (n = 16), moderate (n = 10) and severe (n = 10) groups. **(h)** PCA plot of ILCp showing the contribution of cell surface markers indicated in (g). **(a, c, e, g)** Statistical differences were tested using the Kruskal–Wallis test followed by Dunn's multiple comparisons. Bar graphs are shown as median ± IQR, *P < 0.05, **P < 0.01, ***P < 0.001. Patients with low cell numbers (fewer than 20 events) in the corresponding gate were removed from the analysis. In PCA plots, each dot represents one donor. Deceased patients in the severe group are indicated by a black dot.

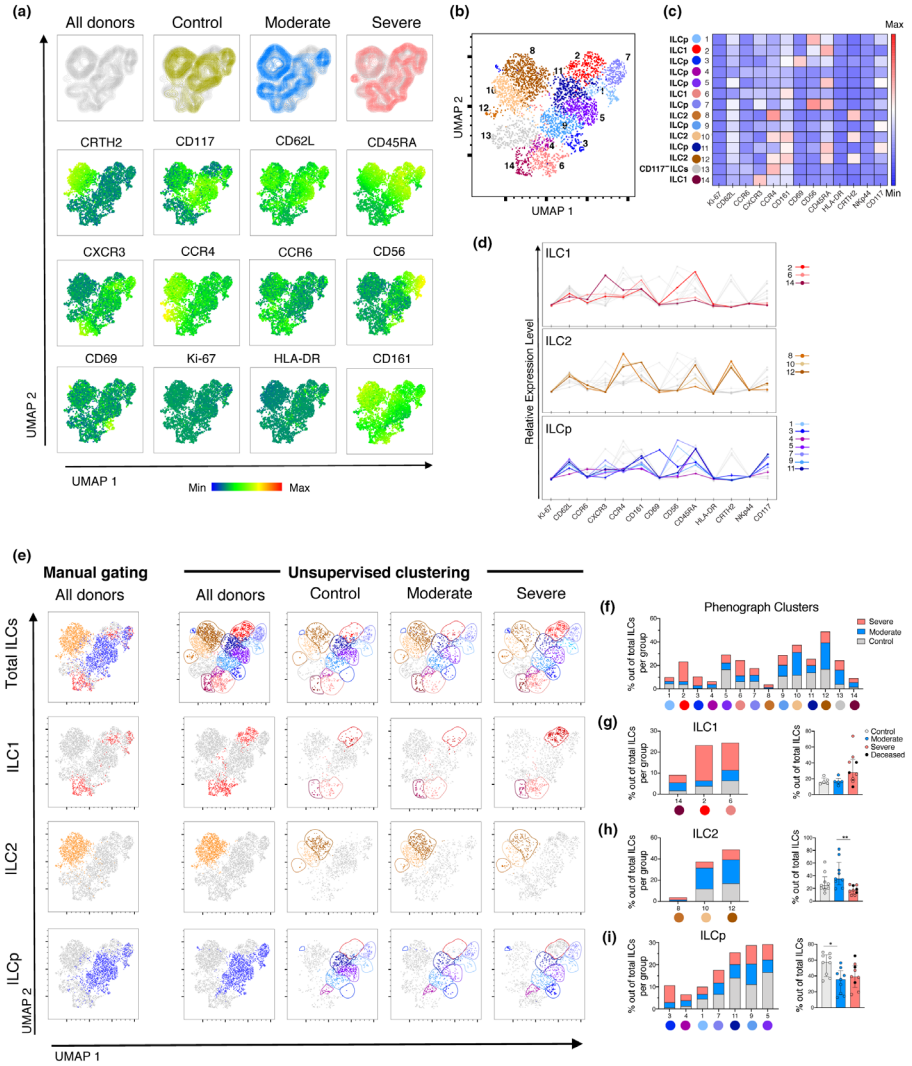

Figure 4. Dimensionality reduction analysis of ILCs in the peripheral blood of COVID-19 patients distinguishes moderate and severe COVID-19 patients. **(a)** Top row: UMAP of total ILCs from control donors and COVID-19 patients (All donors), overlaid by patient groups: control donors (yellow), moderate COVID-19 patients (blue) and severe COVID-19 patients (pink) (from left to right). Middle and bottom rows: UMAP (All donors) coloured according to the fluorescence intensity expression (median) of the indicated phenotypic markers. **(b)** UMAP of the total ILCs overlaid with the 14 clusters identified by Phenograph. **(c)** Heatmap displaying the median of expression of the indicated markers for each Phenograph cluster. Each cluster was assigned an ILC subset identity (ILC1, ILC2, ILCp and CD117^{-} ILC) based on the heatmap and the relative expression levels graph in (d). **(d)** Relative expression level of markers in the Phenograph clusters, grouped by ILC subsets (ILC1, ILC2 and ILCp). Grey lines in each graph are the rest of clusters not belonging to the ILC subset depicted. **(e)** Far left column: manually defined gates of total ILCs and ILC subsets ILC1, ILC2 and ILCp overlaid on the All donors UMAP in **(a)**. Right columns: UMAP of total ILCs overlaid with the 14 ILCs clusters identified by Phenograph and displayed according to patient group (columns) and ILCs subsets (rows). Colours used for the clusters correspond to the colours used in Figure 4b–d. **(f)** Stacked bar graph of the percentage of all the Phenograph-identified clusters out of total ILCs in control donors (grey), moderate (blue) and severe COVID-19 patients (pink). **(g)** Left: stacked bar graph of the percentage of the Phenograph-identified clusters belonging to ILC1 out of total ILCs in controls (grey), moderate (blue) and severe (pink) COVID-19 patients. Right: Percentage of the sum of events corresponding to the ILC1 Phenograph-identified clusters (14, 2, 6) out of total ILCs, in control donors (n = 5), moderate (n = 5) and severe (n = 9) COVID-19 patients. **(h)** Left: stacked bar graph of the percentage of the Phenograph-identified clusters belonging to ILC2 out of total ILCs in control donors, moderate and severe COVID-19 patients. Right: Percentage of the sum of events corresponding to the ILC2 Phenograph-identified clusters (8, 10, 12) out of total ILCs, in control donors (n = 9), moderate (n = 9) and severe (n = 9) COVID-19 patients. **(i)** Left: stacked bar graph of the percentage of the Phenograph-identified clusters belonging to ILCp out of total ILCs in control donors, moderate and severe COVID-19 patients. Right: percentage of the sum of events corresponding to the ILCp Phenograph-identified clusters (3, 4, 1, 7, 11, 9, 5) out of total ILCs, in control donors (n = 9), moderate (n = 9), and severe (n = 9) COVID-19 patients. **(g–i)** Patients with fewer than 10 events per ILC subset (defined by the Phenograph-identified clusters) were excluded from analysis. Statistical differences were tested using the Kruskal–Wallis test followed by Dunn's multiple comparisons test. Bar graphs are shown as median ± IQR, $^{*}P < 0.05$, $^{**}P < 0.01$.

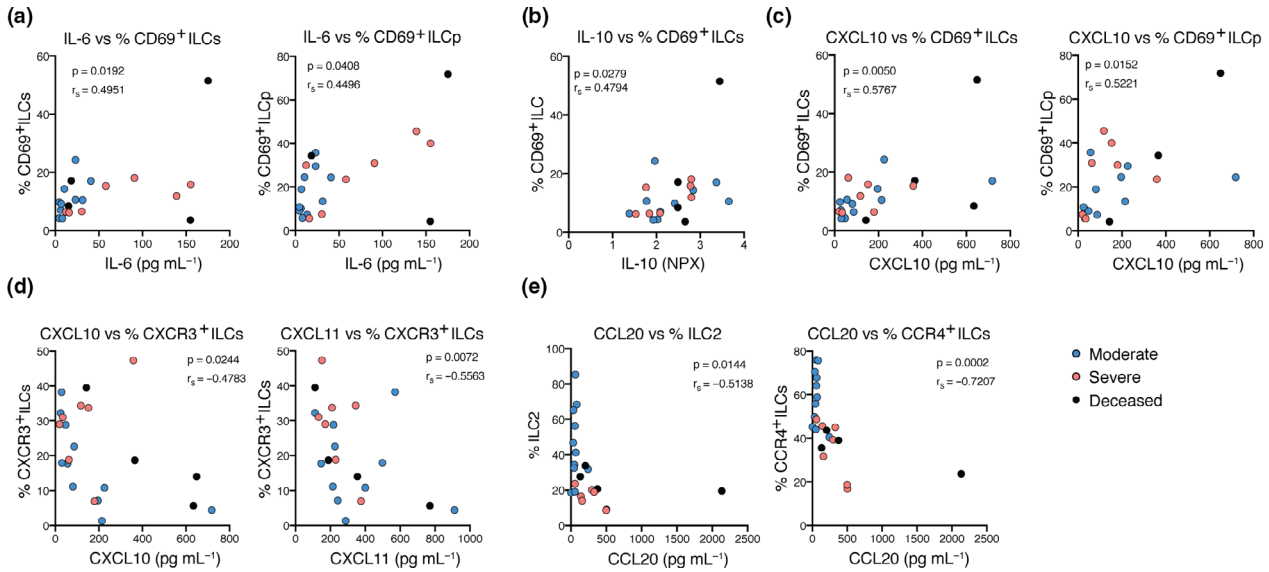

Figure 5. Activation status and homing profile of peripheral blood ILCs associate with inflammation markers in COVID-19 patients. Spearman correlations between **(a)** serum IL-6 levels (pg mL^{-1}) and the percentage of $CD69^+$ ILCs and $CD69^+$ ILCp; **(b)** serum IL-10 relative levels (NPX) and the percentage of $CD69^+$ ILCs; **(c)** serum CXCL10 levels (pg mL^{-1}) and the percentage of $CD69^+$ ILCs and $CD69^+$ ILCp; **(d)** serum CXCL10 and CXCL11 levels (pg mL^{-1}) and the percentage of $CXCR3^+$ ILCs; **(e)** serum CCL20 levels (pg mL^{-1}) and the percentage of ILC2 and $CCR4^+$ ILCs in COVID-19 patients. IL-6, CXCL10, CXCL11 and CCL20 serum absolute levels were measured with Magnetic Luminex Screening assay, and IL-10 relative levels with a proximity extension assay, where data are shown as normalised protein expression (NPX). Blue circles: moderate COVID-19 patients ($n = 11$); pink circles: severe COVID-19 patients ($n = 11$); black circles: deceased severe COVID-19 patients ($n = 4$). $P < 0.05$ was considered statistically significant. r_s: Spearman's rank correlation coefficient.

Uniform Manifold Approximation and Projection (UMAP) analysis confirmed and extended the findings obtained by manual gating in an unsupervised manner. As expected from manual gating, clear differences in ILC composition between controls and COVID-19 patients were observed when overlaying each group to the UMAP containing all concatenated ILC events (Figure 4a, Supplementary figure 2b). Phenograph clustering yielded a total of 14 distinct clusters across patients and controls (Figure 4b). Based on the relative expression of CRTH2, CD117 and CXCR3, clusters were identified as ILC1, ILC2 or ILCp (Figure 4c and d). Thereafter, manually defined ILC subset gates that were overlaid into the UMAP (Figure 4e) showed a similar spatial distribution as the Phenograph-defined clusters belonging to each ILC subset, confirming the precision of the manual gating relative to the unsupervised analysis (Figure 4b).

Next, we assessed each Phenograph-defined cluster. Validating the manual gating, $CCR4^+$ ILC1 (cluster 14) was uniquely present in COVID-19 patients, while two additional $CCR4^{-/lo}$ ILC1 clusters (2 and 6) were overrepresented in severe COVID-19 patients (Figure 4f and g). For ILC2, cluster 8, containing $CCR4^{hi}$ ILC2, was only present in COVID-19 patients and other two $CCR6^+$ ILC2 clusters (10, 12) were accumulated in moderate patients (Figure 4f and h). Corroborating again the findings from manual gating (Figure 3), cluster 3, uniquely present in COVID-19 patients, corresponded to activated ($CD69^+$) ILCp lacking CXCR3 (Figure 4f and i). Furthermore, three ILCp clusters (1, 5 and 7) with an immature phenotype ($CD45RA^{+/hi}/CD62L^{+/hi}$) were reduced in COVID-19 patients as compared with controls (Figure 4f and i), in support of the data obtained by manual gating (Figure 3).

Altogether, the unsupervised analysis revealed clusters specifically accumulated in COVID-19 patients compared to controls and the presence of specific ILC phenotypes that associated to the disease severity. Importantly, several of the findings agreed with those obtained by manual gating. Specifically, we confirmed an increase in the relative frequency of $CD69^+$ ILCp and a decrease in $CXCR3^+$ ILCp in both moderate and severe COVID-19, an increase in ILC2 percentage specifically in moderate COVID-19 and an increased CCR4 expression among ILC1 in the patients.

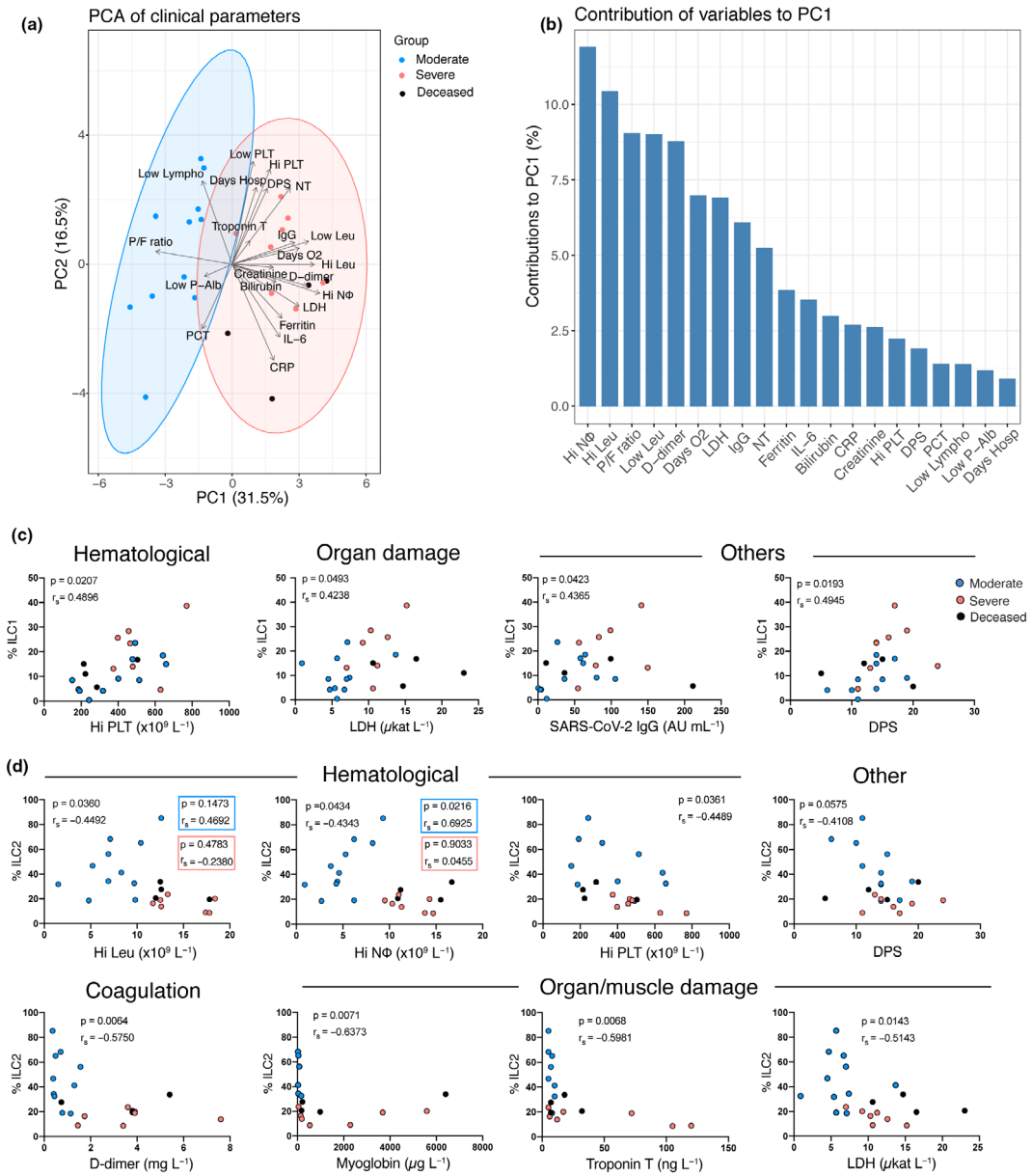

Figure 6. Peripheral blood ILC subsets associate with biochemical and haematological parameters that reflect COVID-19 severity. **(a)** Principal component analysis (PCA) of COVID-19 patients displaying the distribution and segregation of COVID-19 patients according to clinical and laboratory parameters. **(b)** Bar plot showing the percentage contribution of each clinical or laboratory parameter to principal component 1 (PC1). **(c)** Correlation plots between the percentage of ILC1 and the indicated haematological (Hi PLT), organ damage (LDH) and other parameters (SARS-CoV-2 IgG and DPS) in COVID-19 patients (moderate $n = 11$; severe $n = 11$). **(d)** Correlation plots between the percentage of ILC2 and the indicated haematological (Hi Leu, Hi NΦ, Hi PLT and DPS), coagulation (D-dimer), organ damage (myoglobin, troponin T and LDH) and other (DPS) parameters in COVID-19 patients (moderate $n = 11$; severe $n = 11$). Hi NΦ: highest neutrophil count ± 24 h from sampling (f.s.); Hi Leu: highest leukocyte count ± 24 h f. s.; P/F ratio: PaO_2/FiO_2 ratio (mmHg) at sampling; Low Leu: Lowest leukocyte count ± 24 h f. s.; D-dimer: highest D-dimer level ± 24 h f. s.; Days O_2: days of oxygen treatment; LDH: highest lactate dehydrogenase before sampling (b.s); IgG/SARS-CoV-2 IgG: SARS-CoV-2 IgG antibody level; NT: neutralising antibody titres at sampling; Ferritin: highest ferritin level ± 24 h f. s.; IL-6: IL-6 levels at the time of sampling; Bilirubin: highest bilirubin ± 24 h f. s.; CRP: highest C-reactive protein ± 24 h f. s.; Creatinine: highest creatinine ± 24 h f. s.; Hi PLT: highest platelet count b.s; DPS: days post-symptom debut until sampling; PCT: highest procalcitonin ± 24 h f. s.; Low Lympho: Lowest lymphocyte count ± 24 h f. s.; Low P-Alb: lowest P-Albumin ± 24 h f. s.; Days Hosp: days of hospitalisation until sampling. Spearman's rank correlation test was applied for assessing correlations between variables.

To analyse for potential factors involved in the activation and potential recruitment of ILCs to tissues in the COVID-19 patients, we examined correlations between ILCs and a wide array of soluble serum factors (Supplementary figure 4a and b). Based on our findings on altered frequencies of $CXCR3^+$ and $CD69^+$ ILCs in COVID-19 (Figure 3a), we focused on selected chemokines (CCL20, CXCL10 and CXCL11) and factors previously reported to be increased in COVID-19 or other viral respiratory disease: IL-6, IL-10, IL18R1 and PD-L1.[7–9,26–31] Interestingly, we found that the percentage of activated ($CD69^+$) total ILCs and activated ILCp positively correlated with serum IL-6 levels in the COVID-19 patients (Figure 5a). Additionally, the relative levels of the cytokine IL-10 also positively correlated with the levels of $CD69^+$ ILCs in the COVID-19 patients (Figure 5b). Moreover, the percentage of $CD69^+$ total ILCs and ILCp positively correlated with CXCL10 levels in the COVID-19 patients (Figure 5c), suggesting that this chemokine is related to the increase in the percentage of activated ILCs that remain in the circulation of COVID-19 patients.

Furthermore, indicative of dysregulated ILC tissue migration in COVID-19, we observed a negative correlation of CXCL10 and CXCL11 levels (CXCR3 ligands), with the percentage of $CXCR3^+$ ILCs in COVID-19 patients (Figure 5d). Additionally, the percentage of $CCR4^+$ total ILCs and ILC2 negatively correlated with CCL20 (ligand for CCR6) levels (Figure 5e). The latter correlation is in line with the high expression of CCR6 on circulating ILC2.[17]

Of further interest, IL18R1 and PD-L1, involved in type 1 inflammation,[29,32] negatively correlated with the level of $CD45RA^+$ ILCp, suggesting that the inflammatory status of COVID-19 patients may promote maturation, depletion and/or tissue migration of ILCp in the systemic circulation (Supplementary figure 4c).

We next sought to integrate our flow cytometric data with the clinical and laboratory findings from the same patients. Clinical information and laboratory measurements (summarised in Tables 1 and 2) integrated in a PCA clustered the patients on the basis of disease severity (Figure 6a) with several haematological and biochemical factors particularly driving this separation (Figure 6b).

We searched for potentially relevant correlations between ILCs and the clinical and laboratory parameters (Supplementary figure 5). The frequencies of ILC1 and ILC2 correlated with several of the measured parameters, whereas no correlations were found for ILCp frequencies (Supplementary figure 5). The percentage of ILC1 positively correlated with LDH and serum SARS-CoV-2 IgG levels, which were significantly increased in severe COVID-19 patients (Figure 6c, Supplementary figure 1). ILC1 frequencies also positively correlated with parameters that did not differ between the two COVID-19 patient groups, i.e. platelet counts and days post-symptom debut (Figure 6c, Table 1 and 2). The percentage of ILC2, in contrast, was negatively correlated with the leukocyte, neutrophil and platelet count (Figure 6d). Interestingly, high neutrophil levels, which have been described as partial predictors of disease severity,[33] also contributed heavily to the separation between patient groups in the current study (Figure 6a and b). Of note, neutrophils have been found to inhibit ILC2 function, thus preventing allergic airway inflammation.[34] Additionally, the relative frequency of ILC2 correlated negatively with levels of D-dimer, a coagulation factor that has been suggested as a systemic biomarker of disease severity in COVID-19 (Figure 6d).[33,35] Finally, we observed a negative correlation between ILC2 frequencies and organ/muscle damage markers (myoglobin, troponin T, LDH) and the number of days since symptom debut (Figure 6d). These findings suggest that among COVID-19 patients, elevated frequencies of ILC1 and decreased frequencies of ILC2 are hallmarks of COVID-19 patients with a clinical profile associated with severe disease.

DISCUSSION

We report unphysiologically reduced levels of ILCs in the circulation of COVID-19 patients, both in percentage and absolute counts, in line with a recent report,[36] and the overall reduction of peripheral blood lymphocytes described in COVID-19.[6,27,37,38] In addition to the overall ILC depletion, we found major changes in the residual circulating ILC compartment in COVID-19 patients, including altered frequencies of ILC subsets, increased activation and dysregulated migration receptor expression. Our data imply that the circulating ILCs are activated and have differentiated and/or are differentially recruited to tissues, where they may contribute to the anti-viral defence.

Noteworthy, we found decreased circulating ILC2 frequencies in severe but not moderate COVID-19

patients, suggesting that ILC2 may be differentially regulated dependent on severity of disease. Supporting this, the relative frequency of ILC2 in COVID-19 patients correlated negatively with the coagulation factor D-dimer, previously shown to be associated with the development of severe disease[33,35] as well as organ/muscle damage markers, suggesting that low ILC2 levels in COVID-19 patients could be indicative of a more severe disease outcome. Indeed, ILC2 have been shown to have a prominent role in lung tissue repair during influenza A infection in mice.[22] This was achieved through production of the epidermal growth factor-related protein amphiregulin, also shown to be involved in promotion of regulatory T cells and cell survival in hepatitis C virus infection.[39,40] The role for ILC2-derived amphiregulin in lung tissue repair in humans is unknown and deserves further exploration in COVID-19.

In contrast to ILC2, ILCp frequencies were diminished in all COVID-19 patients as compared with controls, suggesting their migration to the site of infection or differentiation into mature ILC subsets in the circulation. This has previously been described in an adoptive transfer mouse model.[18] In support of this hypothesis, both ILC2 and ILCp showed an activated phenotype, based on increased frequencies of $CD69^+$ and/or $HLA\text{-}DR^+$ cells. This is in line with the recent discovery of increased frequencies of $CD69^+$ NK cells in COVID-19.[41] Interestingly, in addition to its known role as an early activation marker, CD69 is also a marker of tissue residency.[42] Thus, the presence of the CD69-expressing ILCs in circulation could also indicate retrograde migration from tissue to circulation after local tissue activation, as recently shown for resident memory T cells.[43] Furthermore, we observed that the CD69-expressing cells in the circulation of COVID-19 patients positively correlated with the levels of IL-6 and IL-10, suggesting that the inflammatory status in these patients could be the driver of ILC activation and/or recirculation. Additionally, these CD69-expressing cells positively correlated with the chemokine CXCL10 in patients. In contrast, $CXCR3^+$ ILCs negatively correlated with CXCR3 ligands CXCL10 and CXCL11, potentially indicating a CXCR3-dependent tissue migration of ILCs in COVID-19. $CXCR3^+$ ILCs include IFN-γ producing ILC1,[11,20] which are accumulated in acute and chronic intestinal inflammation in humans.[11] While ILC1 are essential for clearance of cytomegalovirus in mice,[44] the role for ILC1 in human anti-viral immunity, including COVID-19, remains obscure and requires further exploration. Additionally, as ILC1 were defined as $CD161^+$ cells in our study, future examination of $CD127^+CD161^-CD117^-$ ILC-like cells in COVID-19 is warranted.

Lastly, the phenotypic characterisation of circulating ILCs performed in this study would benefit from additional analyses delineating the functionality of ILCs as well as the impact of the tissue microenvironment to their phenotype and function. Of special interest would be the study of ILCs from tissue resident sites, such as lung and intestine, which have been described as main sites of SARS-CoV-2 infection and shedding.[45–48] We have previously reported increased ILC2 frequencies in the intestine of patients with inflammatory bowel disease[17] and in the lungs of patients with asthma,[49] likely due to their influx from the circulation. In line with this, it is possible that the lower ILC frequencies observed in severe as compared with moderate COVID-19 patients could indicate potential trafficking of ILC2 to inflamed infection sites as previously described in asthma[49] and cystic fibrosis.[50] In striking resemblance with the latter study, we observed the lowest frequencies of ILC2 in patients with the highest serum levels of CCL20, and reduced frequencies of $CCR6^+$ ILC2 in COVID-19 patients. Hence, our data point towards a role for CCL20-mediated recruitment of $CCR6^+$ ILC2 to the lung of COVID-19 patients, where they could contribute to fibrosis.[50] To exhaust this and other possible roles for ILC2 in COVID-19, further studies at the tissue level are required.

In summary, this study provides a phenotypic characterisation of circulating ILCs of COVID-19 patients. We identified that altered frequencies of ILCs correlate with clinical and laboratory parameters linked to COVID-19 disease severity. Lastly, to the best of our knowledge, this is the first comprehensive study of ILCs in the context of a human respiratory viral infection. Thus, these data pave the way for a better understanding of the role of this innate immune cell compartment in other viral infectious diseases.

METHODS

Study participants and sampling

As a part of the Karolinska KI/K COVID-19 Immune Atlas, 23 COVID-19 patients (6 females and 17 males; median age 57 years; age range 18–74 years) positive for SARS-CoV-2 RNA by diagnostic RT-qPCR and hospitalised at the

Karolinska University Hospital (Stockholm, Sweden) were included in the present study. Patients were classified as COVID-19 moderate ($n = 11$) and severe ($n = 12$), based on the peak supplementary oxygen received during hospitalisation until the time of inclusion in the study. The moderate group required low or no supplementary oxygen (low oxygen flow, $\leq$ 15 L min^{-1}), out of whom 8 were hospitalised in the regular ward and 3 in the intensive care unit (ICU). These patients had median ordinal scale of 5 (IQR 4-5) at sampling. The severe group consisted of patients that were hospitalised in the ICU and required mechanical ventilation or extracorporeal membrane oxygenation (ECMO; one patient) provided within an intensive care setting. These patients had a median ordinal scale score of 7 (IQR 7-7) at sampling. This classification was in line with the 8-category ordinal scale described by Beigel *et al*. as well as in the WHO guidelines.[51,52]

Peripheral blood sample from all COVID-19 patients was collected 5–24 days (median 14 days; IQR 5–24 days) after symptom debut and 0–8 days after hospitalisation.

Sixteen donors (6 females and 10 males; median age 54 years; age range between 34 and 69 years), all SARS-CoV-2 IgG seronegative and symptom-free at the day of sampling, were included as a control group for this study. Detailed donor characteristics are summarised in Tables 1 and 2.

This study was approved by the Swedish Ethical Review Authority and conducted according to the Declaration of Helsinki. All patients or next of kin and control donors provided oral and/or written informed consent in line with the ethical approval.

Serum collection and cell isolation from whole blood

Peripheral blood mononuclear cells (PBMCs) from control donors and COVID-19 patients were isolated from heparinised anti-coagulated blood in SepMate tubes (Stemcell Technologies, Vancouver) using gradient density centrifugation, according to manufacturer's instructions. Briefly, 15 mL of Lymphoprep™ (Stemcell Technologies) was pipetted below the SepMate insert and 20 mL of diluted whole blood was dispensed on top. Tubes were centrifuged at 1200 *g* for 10 min. The supernatant including PBMCs was carefully decanted into a new tube, followed by two washes with PBS containing 10% FCS. Platelets were removed by centrifuging the samples at 400 *g* for 10 min. Pellets were resuspended, cells counted and subsequently stained for flow cytometry.

Serum was collected from COVID-19 patients and control donors in BD Vacutainer serum tubes with spray-coated silica (BD Biosciences, San Jose). After coagulation for up to 2 h at room temperature (RT), serum was isolated by centrifugation at 2000 *g* for 10 min and immediately stored at –80°C for later analysis.

Cell staining and flow cytometry analysis

Freshly isolated PBMCs were stained with dead cell marker (Invitrogen, Carlsbad) and fluorochrome-conjugated antibodies directed against intracellular and surface markers (Supplementary table 1) for 20 min at RT in the dark. Cells were washed two times with 150 μL of PBS with 10% FCS. Next, pellets were resuspended in 100 μL of BD FACS Lysing Solution (BD Biosciences) and incubated for 10 min at RT, for cell fixation. After washing with PBS with 10% FCS, cells were permeabilised using 100 μL of BD Perm2 Permeabilizing Solution (BD Biosciences) for 10 min at RT. Subsequently, antibodies were added for intracellular staining and incubated for 30 min at RT in the dark. Cells were then washed with 150 μL of PBS with 10% FCS and incubated in a 1% formaldehyde solution for 2 h, washed and resuspended in PBS containing 10% FCS.

Samples were acquired on a BD LSR Fortessa™. Flow cytometric analysis was performed using FlowJo version 10.6.2 (TreeStar, Ashland).

UMAP analysis

To ensure unbiased manual gating, a blinded analysis was implemented, whereby all FCS3.0 files were renamed and coded by one person and blindly analysed by another person. All samples were compensated electronically, and gatings were based on fluorescent-minus-one (FMO) or negative controls. After all gatings were performed, samples were decoded and statistical analysis between groups and unsupervised analysis was performed. For unsupervised analysis, the following FlowJo plugins were used: DownSample (v.1.1), UMAP (v.2.2), Phenograph (v.2.4) and ClusterExplorer (v.1.2.2) (all FlowJo LLC). First, 133 events per patients were downsampled from the total ILC gate (Supplementary figure 2b). The new generated FCS files were labelled according to control or patient group (moderate or severe COVID-19) and concatenated per group. Subsequently, all groups were taken to the same number of events, by downsampling to the number of events present in the group with the least number of events. The three new FCS files corresponding to control, moderate and severe COVID-19 patients were then concatenated for dimensionality reduction analysis using UMAP. UMAP was run including the markers CRTH2, CD161, CD117, CD69, HLA-DR, Ki-67, CD45RA, CD62L, CCR4, CCR6, CXCR3, CD56, NKp44 and using the following parameters: metric = euclidean, nearest neighbours = 15, and minimum distance = 0.5. Clusters of phenotypically related cells were identified using Phenograph plugin and including the same markers as for UMAP and parameters $k = 30$ and Run ID = auto. Finally, ClusterExplorer plugin was used to study the phenotype of the different clusters and to generate heatmaps of marker expression from those clusters.

Absolute cell counts

Absolute numbers of ILCs in peripheral blood were obtained using BD Multitest™ 6-color TBNK reagents with bead-containing BD Trucount™ tubes (BD Biosciences), according to manufacturer's instructions. Briefly, 50 μL of anti-coagulated whole blood was added into Trucount tubes within 3 h after blood extraction. Then, an antibody mix was added for staining. After 15 min of incubation at RT in the dark, stained whole blood was fixed and red blood cells lysed with 1 × BD FACS Lysing Solution (BD Biosciences) for 2 h at RT. Samples were then fixed with 1% PFA for 2 h prior to acquisition in a FACSymphony A5 (BD

Biosciences) flow cytometer. Absolute ILC cell counts were calculated using the formula:

$$\begin{aligned}&\text{ILC (number per mL)}\\&=\left[\frac{(\#\,\text{lymphocytes events acquired}*\text{total \#beads in tube}*1000)}{(\#\text{beads acquired}*\text{volume of whole blood stained }(\mu L))}\right]\\&*\%\,\text{ILC out of lymphocytes}\end{aligned}$$

ILC1, ILC2 and ILCp absolute counts were calculated using their frequencies relative to total ILCs.

Analysis of serum biomarkers

Heat-inactivated (56°C for 30 min) serum from all patients and controls was analysed for soluble protein biomarkers using proximity extension assay (PEA) technology (Olink AB, Uppsala, Sweden). The samples were analysed using the inflammation (v.3022) panel, including a total of 92 analytes. Data are expressed as normalised protein expression (NPX) values. NPX is an arbitrary unit on a $\log_2$ scale to normalise data to minimise both intra-assay and inter-assay variation.

Additionally, several soluble analytes were also measured in serum or plasma by use of custom made multiplex Magnetic Luminex Screening assays (R&D Systems, Minneapolis), according to the manufacturer's instructions. Serum and plasma were diluted 1:2 prior to multiplex analysis.

Analytes from Olink data and Magnetic Luminex Screening assays that had more than 33% and 25% of missing values, respectively, were excluded from analysis. Left-censored data from the multiplex analysis were imputed using GSimp package[53] in R (v. 3.6.0)[54].

Clinical parameters and serology

Serum samples from all patients and controls were analysed for presence of SARS-CoV-2 antibodies, as recently described.[55]

Micro-neutralisation assay for measurement of neutralising antibody titres was performed as previously described.[56] Briefly, heat-inactivated serum (56°C for 30 min) was diluted twofold starting at 1:10, mixed with an equal volume of 200 TCID50 SARS-CoV-2 (50 μL diluted serum plus 50 μL virus) and incubated for 1 h at 37°C and 5% CO_2. Mixtures were then added to Vero E6 cells and incubated at 37°C 5% CO_2 for four days. Cells were inspected for signs of cytopathic effect (CPE) by optical microscopy. Results were expressed as the arithmetic mean of the reciprocals of the highest neutralising dilutions from the two duplicates for each sample.

Statistical analysis

Statistical analyses were performed using Prism version 8.4.3 (GraphPad Software Inc., San Diego). For comparisons between three unpaired groups, the Kruskal–Wallis test followed by Dunn's multiple comparisons test was used. Correlation analyses were performed using Spearman's rank correlation. Spearman's correlation matrix was generated with R (v.4.0.2) using package corrplot (v.0.84). Statistical differences between the moderate and severe COVID-19 patients or control donors and COVID-19 patients were determined by the two-sided Mann–Whitney *U*-test. *P*-values < 0.05 were considered statistically significant.

Principal component analysis (PCA) was performed in R (v.4.0.2; R Core Team, 2020) using packages Factoextra (v.1.0.7),[57] FactoMineR (v.2.3),[58] RColorBrewer (v.1.1-2)[59] and ggplot2 (v.3.3.2).[60] Data were normalised in R using the *scale* argument within the PCA function. Where data were missing, the values were imputed using package WaverR (v1.0)[61] using 1000 repetitions.

ACKNOWLEDGMENTS

We express our sincere gratitude to all the patients and their families as well as the clinical personnel that helped to carry out the study as part of the Karolinska KI/K COVID-19 Immune Atlas. We also thank the team at the SciLifeLab Plasma Profiling Facility in Stockholm for generating the Olink data. This study was supported by the Knut and Alice Wallenberg Foundation, Nordstjernan AB, Swedish Research Council Vetenskapsrådet (VR), Karolinska Institutet and the SciLifeLab COVID-19 National Program.

CONFLICT OF INTEREST

The authors declare that the research was conducted in the absence of any commercial or financial relationships that could be construed as a potential conflict of interest. HGL is a member of the board of XNK Therapeutics AB and Vycellix Inc.

AUTHOR CONTRIBUTIONS

Marina García: Conceptualization; Data curation; Formal analysis; Investigation; Methodology; Writing-original draft. **Efthymia Kokkinou:** Conceptualization; Data curation; Formal analysis; Investigation; Methodology; Writing-original draft. **Anna Carrasco García:** Conceptualization; Investigation; Methodology; Writing-review & editing. **Tiphaine Parrot:** Conceptualization; Methodology; Writing-review & editing. **Laura M Palma Medina:** Conceptualization; Data curation; Formal analysis; Writing-review & editing. **Kimia T Maleki:** Conceptualization; Methodology; Writing-review & editing. **Wanda Christ:** Conceptualization; Methodology; Writing-review & editing. **Renata Varnaitė:** Conceptualization; Resources; Writing-review & editing. **Iva Filipovic:** Conceptualization; Writing-review & editing. **Hans-Gustaf Ljunggren:** Conceptualization; Funding acquisition; Writing-review & editing. **Niklas Björkström:** Conceptualization; Writing-review & editing. **Elin Folkesson:** Methodology; Writing-review & editing. **Olav Rooyackers:** Conceptualization; Methodology; Writing-review & editing. **Lars I Eriksson:** Conceptualization; Writing-review & editing. **Anders Sönnerborg:** Conceptualization; Writing-review & editing. **Soo Aleman:** Conceptualization; Methodology; Writing-review & editing. **Kristoffer Strålin:** Conceptualization; Investigation; Methodology; Writing-review & editing. **Sara Gredmark-Russ:** Conceptualization; Investigation; Writing-review & editing. **Jonas Klingström:** Conceptualization; Funding acquisition; Investigation;

Supervision; Writing-original draft. **Jenny Mjösberg:** Conceptualization; Funding acquisition; Investigation; Supervision; Writing-original draft.

REFERENCES

1. Alijotas-Reig J, Esteve-Valverde E, Belizna C *et al*. Immunomodulatory therapy for the management of severe COVID-19. Beyond the anti-viral therapy: a comprehensive review. *Autoimmun Rev* 2020; **19**: 102569.
2. Riva L, Yuan S, Yin X *et al*. Discovery of SARS-CoV-2 antiviral drugs through large-scale compound repurposing. *Nature* 2020; **586**: 113–119.
3. Le Thanh T, Andreadakis Z, Kumar A *et al*. The COVID-19 vaccine development landscape. *Nat Rev Drug Discov* 2020; **19**: 305–306.
4. Zhou P, Lou Yang X, Wang XG *et al*. A pneumonia outbreak associated with a new coronavirus of probable bat origin. *Nature* 2020; **579**: 270–273.
5. Chen G, Wu D, Guo W *et al*. Clinical and immunological features of severe and moderate coronavirus disease 2019. *J Clin Invest* 2020; **130**: 2620–2629.
6. Huang C, Wang Y, Li X *et al*. Clinical features of patients infected with 2019 novel coronavirus in Wuhan, China. *Lancet* 2020; **395**: 497–506.
7. Azkur AK, Akdis M, Azkur D *et al*. Immune response to SARS-CoV-2 and mechanisms of immunopathological changes in COVID-19. *Allergy Eur J Allergy Clin Immunol* 2020; **75**: 1564–1581.
8. Mahmudpour M, Roozbeh J, Keshavarz M, Farrokhi S, Nabipour I. COVID-19 cytokine storm: the anger of inflammation. *Cytokine* 2020; **133**: 155151.
9. Mehta P, McAuley DF, Brown M, Sanchez E, Tattersall RS, Manson JJ. COVID-19: consider cytokine storm syndromes and immunosuppression. *Lancet* 2020; **395**: 1033–1034.
10. Vivier E, Artis D, Colonna M *et al*. Innate lymphoid cells: 10 years on. *Cell* 2018; **174**: 1054–1066.
11. Bernink JH, Peters CP, Munneke M *et al*. Human type 1 innate lymphoid cells accumulate in inflamed mucosal tissues. *Nat Immunol* 2013; **14**: 221–229.
12. Klose CSN, Kiss EA, Schwierzeck V *et al*. A T-bet gradient controls the fate and function of CCR6-RORγt$^+$ innate lymphoid cells. *Nature* 2013; **494**: 261–265.
13. Moro K, Yamada T, Tanabe M *et al*. Innate production of T(H)2 cytokines by adipose tissue-associated c-Kit$^+$ Sca-1$^+$ lymphoid cells. *Nature* 2010; **463**: 540–544.
14. Neill DR, Wong SH, Bellosi A *et al*. Nuocytes represent a new innate effector leukocyte that mediates type-2 immunity. *Nature* 2010; **464**: 1367–1370.
15. Price AE, Liang HE, Sullivan BM *et al*. Systemically dispersed innate IL-13-expressing cells in type 2 immunity. *Proc Natl Acad Sci USA* 2010; **107**: 11489–11494.
16. Satoh-Takayama N, Vosshenrich CAJ, Lesjean-Pottier S *et al*. Microbial flora drives interleukin 22 production in intestinal NKp46$^+$ cells that provide innate mucosal immune defense. *Immunity* 2008; **29**: 958–970.
17. Forkel M, VanTol S, Höög C, Michaëlsson J, Almer S, Mjösberg J. Distinct alterations in the composition of mucosal innate lymphoid cells in newly diagnosed and established Crohn's disease and ulcerative colitis. *J Crohn's Colitis* 2019; **13**: 67–78.
18. Lim AI, Li Y, Lopez-Lastra S *et al*. Systemic human ILC precursors provide a substrate for tissue ILC differentiation. *Cell* 2017; **168**: 1086–1100.e10.
19. Mjösberg J, Bernink J, Golebski K *et al*. The transcription factor GATA3 is essential for the function of human type 2 innate lymphoid cells. *Immunity* 2012; **37**: 649–659.
20. Roan F, Stoklasek TA, Whalen E *et al*. CD4$^+$ group 1 innate lymphoid cells (ILC) form a functionally distinct ILC subset that is increased in systemic sclerosis. *J Immunol* 2016; **196**: 2051–2062.
21. Simoni Y, Fehlings M, Kløverpris HN *et al*. Human innate lymphoid cell subsets possess tissue-type based heterogeneity in phenotype and frequency. *Immunity* 2017; **46**: 148–161.
22. Monticelli LA, Sonnenberg GF, Abt MC *et al*. Innate lymphoid cells promote lung-tissue homeostasis after infection with influenza virus. *Nat Immunol* 2011; **12**: 1045–1054.
23. Li BWS, de Bruijn MJW, Lukkes M *et al*. T cells and ILC2s are major effector cells in influenza-induced exacerbation of allergic airway inflammation in mice. *Eur J Immunol* 2019; **49**: 144–156.
24. Kløverpris HN, Kazer SW, Mjösberg J *et al*. Innate lymphoid cells are depleted irreversibly during acute HIV-infection in the absence of viral suppression. *Immunity* 2016; **44**: 391–405.
25. Yudanin NA, Schmitz F, Flamar AL *et al*. Spatial and temporal mapping of human innate lymphoid cells reveals elements of tissue specificity. *Immunity* 2019; **50**: 505–519.e4.
26. Liu F, Li L, Xu M *et al*. Prognostic value of interleukin-6, C-reactive protein, and procalcitonin in patients with COVID-19. *J Clin Virol* 2020; **127**: 104370.
27. Zhang X, Tan Y, Ling Y *et al*. Viral and host factors related to the clinic outcome of the SARS-CoV-2 infection. *Nature* 2020; **583**: 437–440.
28. Maleki KT, García M, Iglesias A *et al*. Serum markers associated with severity and outcome of hantavirus pulmonary syndrome. *J Infect Dis* 2019; **219**: 1832–1840.
29. Schönrich G, Raftery MJ. The PD-1/PD-L1 axis and virus infections: a delicate balance. *Front Cell Infect Microbiol* 2019; **9**: 207.
30. Zalinger ZB, Elliott R, Weiss SR. Role of the inflammasome-related cytokines Il-1 and Il-18 during infection with murine coronavirus. *J Neurovirol* 2017; **23**: 845–854.
31. Harker JA, Godlee A, Wahlsten JL *et al*. Interleukin 18 coexpression during respiratory syncytial virus infection results in enhanced disease mediated by natural killer cells. *J Virol* 2010; **84**: 4073–4082.
32. Dinarello CA, Novick D, Kim S, Kaplanski G. Interleukin-18 and IL-18 binding protein. *Front Immunol* 2013; **4**: 289.
33. Velavan TP, Meyer CG. Mild versus severe COVID-19: laboratory markers. *Int J Infect Dis* 2020; **95**: 304–307.
34. Patel DF, Peiró T, Bruno N *et al*. Neutrophils restrain allergic airway inflammation by limiting ILC2 function and monocyte-dendritic cell antigen presentation. *Sci Immunol* 2019; **4**: eaax7006.

35. Zhou F, Yu T, Du R *et al*. Clinical course and risk factors for mortality of adult inpatients with COVID-19 in Wuhan, China: a retrospective cohort study. *Lancet* 2020; **395**: 1054–1062.
36. Kuri-Cervantes L, Pampena MB, Meng W *et al*. Comprehensive mapping of immune perturbations associated with severe COVID-19. *Sci Immunol* 2020; **5**: eabd7114.
37. Qin C, Zhou L, Hu Z *et al*. Dysregulation of immune response in patients with coronavirus 2019 (COVID-19) in Wuhan, China. *Clin Infect Dis* 2020; **71**: 762–768.
38. Wang F, Nie J, Wang H *et al*. Characteristics of peripheral lymphocyte subset alteration in COVID-19 pneumonia. *J Infect Dis* 2020; **221**: 1762–1769.
39. Pei R, Chen H, Lu L *et al*. Hepatitis C virus infection induces the expression of amphiregulin, a factor related to the activation of cellular survival pathways and required for efficient viral assembly. *J Gen Virol* 2011; **92**: 2237–2248.
40. Yuan CH, Sun XM, Zhu CL *et al*. Amphiregulin activates regulatory T lymphocytes and suppresses $CD8^+$ T cell-mediated anti-tumor response in hepatocellular carcinoma cells. *Oncotarget* 2015; **6**: 32138–32153.
41. Maucourant C, Filipovic I, Ponzetta A *et al*. Natural killer cell immunotypes related to COVID-19 disease severity. *Sci Immunol* 2020; **5**: eabd6832.
42. Kumar BV, Ma W, Miron M *et al*. Human tissue-resident memory T cells are defined by core transcriptional and functional signatures in lymphoid and mucosal sites. *Cell Rep* 2017; **20**: 2921–2934.
43. Fonseca R, Beura LK, Quarnstrom CF *et al*. Developmental plasticity allows outside-in immune responses by resident memory T cells. *Nat Immunol* 2020; **21**: 412–421.
44. Weizman OE, Adams NM, Schuster IS *et al*. ILC1 confer early host protection at initial sites of viral infection. *Cell* 2017; **171**: 795–808.e12.
45. Cheung KS, Hung IFN, Chan PPY *et al*. Gastrointestinal manifestations of SARS-CoV-2 infection and virus load in fecal samples from a Hong Kong cohort: systematic review and meta-analysis. *Gastroenterology* 2020; **159**: 81–95.
46. Lamers MM, Beumer J, van der Vaart J *et al*. SARS-CoV-2 productively infects human gut enterocytes. *Science* 2020; **369**: 50–54.
47. Schaefer IM, Padera RF, Solomon IH *et al*. In situ detection of SARS-CoV-2 in lungs and airways of patients with COVID-19. *Mod Pathol* 2020; **33**: 2104–2114.
48. Xiao F, Tang M, Zheng X, Liu Y, Li X, Shan H. Evidence for Gastrointestinal Infection of SARS-CoV-2. *Gastroenterology* 2020; **158**: 1831–1833.e3.
49. Winkler C, Hochdörfer T, Israelsson E *et al*. Activation of group 2 innate lymphoid cells after allergen challenge in asthmatic patients. *J Allergy Clin Immunol* 2019; **144**: 61–69.e7.
50. Schulz-Kuhnt A, Greif V, Hildner K *et al*. ILC2 lung-homing in cystic fibrosis patients: functional involvement of CCR6 and impact on respiratory failure. *Front Immunol* 2020; **11**: 691.
51. Beigel JH, Tomashek KM, Dodd LE *et al*. Remdesivir for the treatment of Covid-19 — preliminary report. *N Engl J Med* 2020; **383**: 992–993.
52. Coronavirus disease (COVID-19). https://www.who.int/emergencies/diseases/novel-coronavirus-2019.
53. Wei R, Wang J, Jia E, Chen T, Ni Y, Jia W. GSimp: a Gibbs sampler based left-censored missing value imputation approach for metabolomics studies. *PLoS Comput Biol* 2018; **14**: e1005973.
54. R Core Team. *R: a language and environment for statistical computing*. R Foundation for Statistical Computing, Vienna, Austria. https://www.r-project.org/
55. Sekine T, Perez-Potti A, Rivera-Ballesteros O *et al*. Robust T cell immunity in convalescent individuals with asymptomatic or mild COVID-19. *Cell* 2020; **183**: 158–168.e14.
56. Varnaitė R, García M, Glans H *et al*. Expansion of SARS-CoV-2-specific antibody-secreting cells and generation of neutralizing antibodies in hospitalized COVID-19 patients. *J Immunol* 2020; **205**: 2437–2446.
57. Kassambara A, Mundt F. factoextra: extract and visualize the results of multivariate data analyses. R package version 1.0.7. https://cran.r-project.org/web/packages/factoextra/index.html
58. Lê S, Josse J, Husson F. FactoMineR: an R package for multivariate analysis. *J Stat Softw* 2008; **25**: 1–18.
59. Neuwirth E. RColorBrewer: ColorBrewer palettes. R package version 1.1-2. https://cran.r-project.org/web/packages/RColorBrewer/index.html
60. Wickham H.ggplot2: elegant graphics for data analysis. https://ggplot2.tidyverse.org/
61. Cheronet O, Finarelli JA. WaverR: data estimation using weighted averages of multiple regressions. https://cran.r-project.org/web/packages/WaverR/index.html

Supporting Information

Additional supporting information may be found online in the Supporting Information section at the end of the article.